# Influence of Hot Rolling Finishing Temperature on Texture and Ridging Resistance in Stabilized Ferritic Stainless Steels

Suresh Kodukula*, Heikki Kokkomäki, Esa Puukko, David Porter, Jukka Kömi

Suresh Kodukula*, Heikki Kokkomäki, Esa Puukko
Tornio Research Center, Outokumpu Stainless Oy,
Terästie 1, 95490 Finland

Emeritus Prof. David Porter
Centre for Advanced Steels Research, Faculty of Technology, University of Oulu
90014 Oulu, Finland

Prof. Jukka Kömi,
Centre for Advanced Steels Research, Faculty of Technology, University of Oulu
90014 Oulu, Finland

Keywords: Hot rolling, cold rolling, texture, hot rolling finishing temperature, ridging



A systematic study has been conducted on a 17% Cr dual stabilized ferritic stainless steel (FSS) to study the evolution of texture during hot-rolling and its effect on ridging resistance after cold-rolling and annealing. Hot rolling was carried out on a 4-high laboratory rolling mill with finishing temperatures in the range 1000 °C to 810 °C to cover the evolution of micro-texture under both conventional hot-rolling conditions and when using low finishing temperatures. Subsequently, the hot-rolled coils were cold rolled and annealed to the same final thickness. The microtextures of the samples were evaluated at each process step using scanning electron microscopy combined with electron backscattered diffraction (SEM-EBSD). Lowering the hot rolling finishing temperature resulted in the formation of intragranular shear bands, which strengthened the γ-fiber in the texture after subsequent annealing of the hot-rolled material. After cold rolling to a reduction of 78 % followed by final annealing, the micro-texture in the final product correlates with the micro-texture

This article has been accepted for publication and undergone full peer review but has not been through the copyediting, typesetting, pagination and proofreading process, which may lead to differences between this version and the Version of Record. Please cite this article as doi: 10.1002/srin.202000695.

after hot rolling. The resistance to ridging in stabilized FSS improved by lowering the finishing temperature during hot rolling. This study shows the importance of the hot rolling process conditions in improving the texture inherited from the casting of FSS.

## 1. Introduction

Ferritic stainless steels (FSS) are used in a wide variety of applications such as kitchenware, home appliances, elevator panels, automotive exhaust systems and white goods, due to their combination of formability, weldability and excellent corrosion resistance. FSS, especially with high chromium contents, are good alternatives to the highly alloyed austenitic steels, which are more expensive primarily due to their nickel content. However, FSS can be prone to a surface defect known as ridging that can occur as a result of sheet forming operations. Ridging leads to a diminished surface quality and extra polishing costs in the manufacturing of the final product. Ridging appears as surface corrugations which develop when the steel is stretched or deep drawn. The height differences between the ridges and adjacent valleys are in the range of 20-50 μm [1-14]. In early research, factors like segregation of alloying elements such as chromium, molybdenum or carbon were associated with the formation of ridging [15–18], but now it is well established that ridging is associated with anisotropic plastic deformation caused by colonies of different crystal orientations.

The ridging phenomenon in FSS is closely related to the final texture inherited from columnar solidification during continuous casting process. An increase in the ratio of equiaxed to columnar grains in cast slabs leads to a significant improvement in ridging resistance [19–22]. As there is no austenite-ferrite phase transformation, which would affect the final texture in stabilized high-chromium FSS, the harmful columnar texture can only be altered by deformation and recrystallization during the hot rolling process. Kodukula et al [22] reported that under conventional hot rolling conditions a FSS slab structure with a low equiaxed grain ratio leads to severe ridging and that even

intermediate annealing cannot improve ridging resistance. The texture of the final cold-rolled and annealed product is known to be inherited from the texture after hot rolling and therefore, in order to achieve good surface quality and formability, the texture of the hot-rolled coil should be optimized with respect to the later process stages [13].

A positive effect of lowering hot rolling finishing temperature to 750°C has been observed in stabilized 21% Cr and 17% Cr FSS. A positive effect of lowering the hot rolling finishing temperature in low-carbon and interstitial-free steel has also been observed and attributed to the formation intragranular shear bands [23,24]. However, Sawatani et al. [25] suggested that the positive effect was caused by a change in the precipitation behavior with finishing temperature and not the formation of intragranular shear bands. Mehtonen et al. [26] studied the hot deformation behavior of 21% Cr dual Ti-Nb stabilized FSS steel under multi-pass deformation conditions simulating those during Steckel mill rolling. They reported that lowering the hot deformation temperature of the third, i.e. final, pass from 800°C to 650°C reduced the sub-grain size, increased the flow stress. and caused the formation of intragranular grain shear bands in grains belonging to the γ-fiber. Lu et al .[27] studied the effect of asymmetrical hot rolling and reported that shear band density is proportional to the roll speed ratio, and that the texture tends to be more uniform with a weaker γ-fiber.

Other measures related to hot rolling have also been suggested to overcome the problems caused by columnar grains in FSS castings such as 1) applying heavy roughing deformation with long inter-pass times to achieve complete recrystallization [28,29], 2) lowering the finishing rolling temperature, or even warm rolling, to promote the formation of shear bands [24,26,27], 3) intermediate annealing during cold rolling [11,30], and 4) asymmetrical cold rolling or cross-rolling at 45° to with respect to the normal direction to improve the distribution of texture components [31,32]. Some of these techniques are, however, difficult and costly to implement on an industrial scale, by either reducing

productivity or reducing energy efficiency. However, improvement of the overall texture is not sufficient to guarantee high ridging resistance: uniformity of the texture on the microscale is required, i.e. lack of grain clustering with orientations <001>//ND and (110)//RD. Most earlier studies have been focused on improving the extent of recrystallization and the texture during hot rolling but have not included the effect of subsequent cold rolling and annealing on ridging. The present study was carried out to clarify the effect of hot rolling finishing temperature on the ridging resistance of the final cold-rolled and annealed sheet in the case of a 17% Cr dual Ti-Nb stabilized FSS.

## 2. Materials and Methods

### 2.1 Materials

EN 1.4509/ASTM 441 dual stabilized with titanium and niobium was produced by Outokumpu Stainless using an electric arc furnace (EAF) followed by treatment in an argon oxygen decarburization (AOD) converter. The liquid steel was further refined in a ladle furnace, where the titanium and niobium were added. Once, the final target composition and temperature was reached, the steel melt is transferred to continuous casting platform for casting into slabs 1250 mm wide and 170 mm thick. For macrostructural studies, a slab sample was cut between the 2$^{nd}$ and 3$^{rd}$ slabs where the casting speed has stabilized. Its chemical composition is given in Table 1. The 170 mm thick slab was re-heated in a walking beam furnace to 1150 °C for 150 min and rough rolled into a transfer bar 25 mm thick using a 4-high reverse roughing mill. A sample from the transfer bar was taken for further investigations in the laboratory.

### 2.2 Experimental

The slab sample was cut in 200 mm wide pieces across the whole slab thickness to allow examination of the casting structure on a section perpendicular to the casting direction. The macrostructure was

revealed by grinding and polishing with 10 μm and 6 μm grit and etching in aqua regia, i.e. a mixture of nitric acid ($HNO_3$) and hydrochloric acid (HCl). The equiaxed grain ratio (EGR) was calculated as the ratio of the total thickness of the equiaxed zone to the slab thickness [21].

Laboratory hot rolling trials were carried out using a pilot reversible 4-high Fröhling mill. Prior to laboratory hot rolling, transfer bar samples with the dimensions 500 x 300 x 25.5 mm (RD x TD x ND) were re-heated to 1100 °C and held for 60 minutes in a chamber furnace for homogenization. Laboratory hot rolling was carried out in four different temperature ranges and the finishing rolling temperatures (FRT), i.e. the temperatures during last pass, were approximately 1000, 930, 870 and 810 °C and no lubrication is used. The temperature during hot rolling was controlled with the aid of roller hearth furnaces located on both sides of the rolling mill. Five hot rolling reductions in the sequence 30%, 30%, 25%, 25% and 20% resulted in a final nominal thickness of 6.0 mm. Laminar cooling was applied after the last pass and cooled to room temperature. The laboratory hot rolling process was designed to simulate the actual conditions encountered in production where the transfer bar is hot reduced in a Steckel mill followed by a Tandem mill, where the usual finishing temperatures are around 950 °C. No practical problems were encountered by the application of lower finish rolling temperatures: the increase in the rolling load was moderate and no edge cracking occurred. The laboratory hot-rolled sheets/bands were annealed for 90 s at 980 °C and air cooled followed by pickling in an acid mixture containing hydrofluoric acid (HF) and nitric acid (HNO3) at 40 °C for 5 min. Annealing after hot rolling improves the homogeneity of the microstructure and distribution of precipitates in the coils before cold rolling and annealing. Coil inhomogeneities together with the increased hardness brought about by low finish rolling temperatures can lead to failures during cold rolling. After annealing and pickling, the 6 mm thick white-hot bands (WHB) were cold rolled with a reduction of approximately 78 % to approximately 1.2 mm using a 2-high reversing mill at the University of Oulu. The cold-rolled sheets were annealed at 1000 °C for 30s and pickled at

40 °C for 5 min in the above-mentioned mixed acid bath. A schematic representation of the laboratory rolling schedules is shown in **Figure 1.** The hot rolling parameters and thicknesses of the samples after hot and cold rolling are given in **Table 2.**

Specimens were cut from all the hot bands in the hot-rolled condition after pre-annealing and after cold rolling and annealing. Microtexture measurements were done by using electron backscatter diffraction (EBSD) in a scanning electron microscope (SEM, LEO 1450VP) at 20 kV with a step size of 1.5 µm. Data acquisition was conducted on cross-sections parallel to the RD-ND and TD-ND planes, i.e. the plane normal to the RD direction. (RD is rolling direction, ND is the sheet normal direction and TD is the transverse direction, i.e. the direction perpendicular to the other two directions). The EBSD measurements were used to generate texture data using the Oxford HKL acquisition and analysis software. Often orientation density function (ODF's) obtained from X-ray diffraction pole figures have been preferred for overall texture measurements; however, Hutchinson et al [33] were of the opinion that EBSD results can provide a better texture evaluation provided the probed area is large enough. In this study, the ODF's are calculated using EBSD data obtained from large areas. Ridging tests were performed on the final sheet products with samples measuring 300 mm along RD and 100 mm along TD by applying 15 % elongation along RD in a tensile testing machine equipped with special grips. The unfiltered 2D raw surface profile after the ridging tests was measured using a non-skidded bench-top 2D stylus profilometer Zeiss Surfcom 2000 SD3 with a stylus tip radius of 2 µm. This raw profile was filtered to calculate the ridging index (RI), which is a unique index taking into account the height of the profile and the spacing between the ridges [6]. The dimensionless RI is then defined as the product of Rz in µm and the peak count Pc in $mm^{-1}$:

$$RI = Rz\ [\mu m] \times Pc\ [mm^{-1}]. \quad (1)$$

## 3. Results & Discussion

3.1 Macrostructure of slab sample and micro-texture of transfer bar

Figure 2 shows the macrostructure of the slab, which mostly comprises columnar grains of <001>//ND orientations giving an equiaxed grain ratio of only 12%. Ridging is known to result from columnar solidification during continuous casting and it has been shown that an increase in the equiaxed grain ratio leads to significant improvements in ridging resistance [22]. An inverse pole figure (IPF) map of a TD-ND plane of the transfer bar is shown in Figure 3a and the location of the mapped area is given in Figure 3b. The EBSD measurements were conducted near the centerline of the sample, but offset somewhat so as to include some of the columnar grains that can been seen in Figure 2. In the IPF maps, red denotes grains orientated with <001>//ND (cube-on-face) and blue grains with <111>//ND. The IPF map indicates that the center of the transfer bar was mostly in the deformed state. Away from the centerline, a small fraction of newly recrystallized grains can be observed. To give a quantitative description of the texture, an orientation density function (ODF) was calculated from the EBSD data by considering each orientation g = {$\phi_1$, $\phi$, $\phi_2$} to have a half scatter width of 5° in Euler space. Figure 3c shows the $\Phi_2$=45° section of the resultant ODF. The as-received transfer bar has the strongest texture component intensity, i.e. f(g) = 6, at {001} <110>, which is inherited from the casting structure.

3.2 Texture evolution during hot rolling

During thermo-mechanical treatments, stabilized FSS undergoes rapid dynamic recovery without any γ/α phase transformation or dynamic recrystallization. Furthermore, the grains with {001} <110> orientations do not easily recrystallize during annealing due to their low Taylor factor and strong tendency to recovery[34–36]. It is known that during hot rolling, surface layers are subjected to heavy redundant shear deformation, which provides an enough driving force to break down the columnar grains near the surface by recovery and recrystallization. However, the interior portion of the material is subjected to plane strain compression, which is unable to break down the coarse columnar

grains. After rolling, the deformed grains remain in the same crystallographic orientation. Microtextures as seen on the RD-ND plane of the hot-rolled and water-cooled samples are presented in Figure 4. It is evident that the hot rolling finishing temperature affects the texture: the textures of the conventionally hot-rolled samples having high finishing temperatures (A and B) are significantly different from those having lower FRT (Samples C and D). Sample A, with FRT at 1000 °C, has been dynamically recovered (Figure 4a), whereas the samples with FRT at 930, 870 and 810°C were in the deformed state, with the degree of deformation increasing considerably as FRT decreases. Sample B is partially recovered, while samples C and D, show intragranular shear bands aligned at 30-35° to the rolling direction. Figure 5 shows the ODFs of the BHB samples. Sample A (Figure 5a) has a strong texture component {001} <110> (cube orientation) with the highest texture intensity f(g) = 8.2. The deformation texture component {001} <110> of α-fiber is highest in sample B, although {111} <110> along the γ-fiber started appearing with very low intensity in sample B (Figure 4b). The total texture intensity further reduced in the samples C and D and the texture components {111} <110> intensity also increased along the γ-fiber.

Figure 6 shows IPFs of the annealed samples after hot rolling. All the samples are completely recrystallized except sample A, which still has deformed grains in the centerline, that have not undergone complete recrystallization process during hot rolling.

The average grain sizes of samples A, B, C and D were 120, 108, 81, and 72µm respectively in hot rolled and annealed condition. Lower the finishing temperature during the hot rolling, the average grain size is decreased which indicates that the recrystallization index was increased. The recrystallized textures are also like the deformed textures and the samples C and D have a larger proportion of grains with <111>//ND orientation compared to the samples A and B. Therefore, hot rolling at lower temperatures lead to a more beneficial rolling texture, favorable for the development of the <111>//ND γ-fiber recrystallization texture during the subsequent annealing of the hot-rolled

material. The <111>//ND texture is known to improve the forming properties and increases the resistance towards ridging.

3.3 Texture evolution during cold rolling and annealing

IPFs of the samples after cold rolling and annealing are presented in Figure 7. All the samples have undergone the same amount of cold reduction after hot rolling and annealing. The IPFs cover the whole thickness of the cold rolled sheets. Unlike during pre-annealing, the centerline of sample A completely recrystallized during the final annealing. As it can be observed from the respective ODFs, all the samples consisted grains with <111>//ND orientations in the centerline, but their volume fraction varied greatly increasing from sample A to D.

For samples A and B, the grains near the surface are predominantly oriented with <110>//RD and (100)//ND, which belong to the α-fiber. Compared to samples C and D, grains with <001>//ND orientations are more frequent in samples A and B. Such grains tend to be grouped into colonies in A and B while in C and D such orientations are homogenously spread across the thickness and width of the sample. From the ODFs of the samples presented in Figure 8, it can be observed that the intensity of the γ-fiber orientation {112} <111> and (554) <225> increases through the series A to D while the strength of the α-fiber <110>//RD orientations has weakened along with the <001>//ND (cube) orientation. The maximum texture intensity in the sample A is 2 at the orientation (112) [131] and sample B maximum texture intensity is 2.7 at the orientation along the {112} <111> along the γ-fiber. The maximum texture intensities of sample C and D are further increased along the γ-fiber to 3.7 and 4.5. Interestingly, the Goss orientation {110} <001> is also strengthened after cold rolling and annealing. The strength of the Goss orientation is highest in sample D and lowest in sample A. The amount of reduction during cold rolling being the same on all the samples, the changes in texture

are directly correlated to the finishing rolling temperature during the hot rolling. Lower the hot rolling finishing temperature, stronger the <111>//ND orientations.

3.4 Surface ridging and mechanical properties

The mechanical properties of the cold-rolled and annealed samples are tabulated in Table 3 together with surface profile characteristics after the ridging test. There are no substantial differences in the mechanic properties of the samples, but ridging performance varies greatly. The surface profiles of all the samples after 15% elongation along RD are shown in Figure 9. The severity of ridging decreases systematically through the series A→B→C→D. The ridging index (RI) and ridging height of sample A are 5.62 and 25.56 μm respectively, whereas the values of RI and Rz are 1.25 and 12.52 μm respectively for sample D, which has the highest resistance towards ridging. The ridging indices are directly correlated to the finishing rolling temperature during hot rolling. Ridging height is decreased substantially in sample D by 50% compared to sample A, reducing the hot rolling finishing temperature from 1000 °C to 810 °C.

3.5 Effect of hot rolling temperature

The hot rolling process plays a key role in modifying the solidification structure of FSS. The misorientation distributions of the grains after hot rolling and annealing are shown in Figure 10. Sample A has the highest frequency of low-angle boundaries with approximately 50% higher in the low angle boundary range than the sample D, indicating that the hot rolled structure was primarily only recovered after deformation, with relatively few recrystallized grains. The high angle grain boundaries among the samples (>15°) consistently increased in samples with lowering the hot rolling finishing temperature. The EBSD images of the samples reveal the same that the degree of recrystallization increased among the samples from A to D with decreasing the finishing rolling temperature. Micro-texture images in the hot-rolled conditions showed that shear bands are

frequent in samples C and D, less frequent in B and almost entirely absent from A (Figure 4). Barnett and Jonas et al. [37] found that during warm rolling of IF steels (known as ferrite rolling) between 700 °C and ambient temperature with a 65% reduction and the deformation structures consisted of many shear bands. In these studies, the shear bands were present in the IF steels irrespective of rolling temperature, whereas in low carbon steels, shear bands appeared in the majority of the grains below ~300 °C but in very few grains above 550 °C. Quadir et al. [38] investigated the formation of shear bands in cold-rolled IF steels using transmission electron microscopy (TEM). Thick shear bands are produced by a relative shear displacement of two thin shear bands which involved rigid body rotation in addition to the misorientation produced by the pair of thin shear bands. The thin shear bands have low-angle (< 10°) crystallographic boundaries with the matrix, whereas the thick shear bands are bound by high-angle (> 15°) boundaries. Also, the thick shear bands are 5-7 times thicker than the thin shear bands, which are only 0.1-0.3 μm in thickness. Shear bands are known to provide nucleation sites for recrystallization [38].

As FSSs possess high stacking fault energy (SFE), the dislocations can cross-slip and climb relatively easily at high temperatures resulting in a high dynamic recovery rate. However, as the deformation temperature decreases, dynamic recovery becomes slower. Barnett and Jonas [34] suggested that dislocation density is the main driving force for recrystallization. They proposed that the increase in dislocation density during hot rolling is linearly proportional to square of the hardness difference between the as rolled and fully recrystallized specimens. Their measurements suggested that the dislocation density increases by a factor of four when the FRT drops from 950 to 750 °C and further confirmed by TEM observations that the dislocation density was higher in the shear bands. Mehtonen et al. [26,39] reported that the static recrystallization of FSS during the inter-pass times had a randomizing effect on the texture, even though the α-, γ- and ε-fibers were always present. Their studies showed that lowering the temperature of the final pass from 950 °C to 800 °C and further to

650 °C led to a significant increase in the flow stress and caused the formation of shear bands in grains belonging to the γ-fiber. The present results also agree with reported studies [26,37–39] on FSSs that shear bands have a strong influence on microstructure development during annealing after hot rolling. Grains with shear bands could be subdivided into much smaller misorientation cells, causing more fragmentation resulting in more recrystallized grains. The misorientation distribution plot of hot rolled annealed samples and the EBSD images (Figure 6 and 10) indicate the same. The studied ferritic stainless steel is dual stabilized to prevent sensitization by binding carbon in (TiNb)(CN) particles. Ti forms coarse TiN and Ti(CN) particles already in the molten steel [22,40–43]. The precipitation of C and N continues at high temperatures in the solid phase such that most of the C and N are removed from the matrix by the beginning of the hot deformation. Intermetallic phases such as Laves, Chi and Sigma can precipitate in the course of hot rolling. However, in the present steel, the absence of Mo means that such precipitation takes several hours below 1000 °C and is not encountered during the steel processing [24,26]. Large non-deformable particles enhance nucleation of new grains during recrystallization, and the coarse TiN particles have been observed to induce recrystallisation in earlier studies on a similar steel to the present [24,26,44]. Soaking prior to hot rolling involved holding for 60 mins at 1100 °C. Thermodynamic calculations indicate that (TiNb)(CN) remains undissolved at that temperature so that no reprecipitation of fine precipitates is expected during hot rolling.

3.6 Effect of final annealing and cold rolling and ridging

Final annealing is one of the most important ways to control the final microstructure and texture of sheet steels. Recrystallization kinetics, final microstructure and texture depend on the structure and texture of the cold-rolled sheet material [40]. Recrystallization of the cold-rolled material begins with rapid recovery into well defined, but inhomogeneous, sub-grain structure. Sinclair et al [35] reported that the substructure in 50% cold-rolled steel is banded with two distinct sub-grain morphologies

corresponding depending on the original grain orientation. Grains with orientations {001} <110> and {112} <110>, belonging to the α-fiber, tend to have larger a sub-grain size and smaller misorientations compared to {111} <110> and {111} <112> type grains, which belong to the γ-fiber.

The microtexture results obtained in the final annealed samples are in line with earlier observations [13] as the γ-fiber is largely inherited from the hot rolling texture and has been strengthened in the sub-surface layers. The misorientation distributions of the cold-rolled and annealed samples are shown in Figure 11. The trend is similar to that of hot-rolled and annealed samples in terms of the frequency of low-angle boundaries (0-15°) which are associated with recovery in grains with α-fiber orientations. This confirms that the orientations of the final cold-rolled structure are largely inherited from the texture after hot rolling and indicates that control of the hot rolling parameters is crucial with respect to altering the columnar grain structure to improve the final texture of stabilized ferritic stainless steels.

The effect of finish rolling temperature on the intensities of the main components of the α- and γ-fibers and ε-fibers of the final annealed and pre-annealed materials is shown in Figure 12. In the hot-rolled and annealed samples, the <100>//ND components were highest in sample A followed by B, C and D, while the opposite trend is seen with the γ-fiber components. The presence of <100>//ND grains in samples A and B was apparent in the EBSD-IPFs (Figure 7). When the hot rolling FRT is 1000 °C, the orientation {001} <110> is dominant in the hot-rolled and annealed sample A, but the texture is more random as the FRT is lowered. In sample D with the lowest FRT (810 °C), the texture components belonging to the α- and γ-fibers have similar intensities. In the final annealed samples, the {111}//ND intensities are 3 to 3.5 times higher when FRT is at its lowest compared to its highest, where the [111}//ND intensities are equal to the <110>//RD intensities. As can be observed from the ε-fiber in Figure 12, the texture component {554} <225> and the Goss orientation {110} <001>

increased as the hot rolling finishing temperature decreased. The presence of a strong Goss component in a stabilized stainless steel after the first stage of a two-stage cold rolling process was reported by Rodrigues et al [41]. In that study, as here, the presence of the Goss component is probably due to the use of laboratory cold rolling without lubrication, which increases the near-surface shear strain during rolling[42,43]. The texture component in samples A and B (Figure 7a, 7b) in the final annealed condition, grains with orientations <110>//RD were present in clusters across the width and thickness of the samples. Grains in <110>//RD orientations have a lower plastic strain ratio than grains in other orientations, and when they are clustered the material is prone to ridging [4,34,44,45].

## 4. Summary and Conclusions

The effect of hot rolling finishing temperature on micro-texture distribution and evolution in titanium-niobium stabilized ferritic stainless steels has been studied at various thermomechanical stages from the rough-rolled state through hot rolling, intermediate annealing, cold rolling and final annealing to understand how the finish rolling temperature influences the ridging resistance of the finished cold-rolled and annealed sheet material. Lowering the hot rolling finishing temperature below that conventionally used led to the formation of in-grain shear bands which promoted recrystallization during the subsequent annealing process. When the hot rolling finishing temperature is high like that used conventionally in production of FSSs, after hot rolling and annealing, the centerline is in a deformed and recovered state, whereas when the hot rolling finishing temperature is lowered, the frequency of sub-grain boundaries is increased and there is an increase in the incidence of grains belonging to <111>// ND orientations, which is the result of in-grain shear bands strengthening the γ-fiber after the intermediate annealing treatment. The severity of ridging in the cold-rolled and annealed finished sheet material is proportional to the hot rolling finishing

temperature. The ridging height is reduced by approximately by 50% when the finish temperature of hot rolling is reduced from 1000 °C to 810 °C.

## Acknowledgements

The authors gratefully acknowledge the support of Outokumpu Stainless Oy in providing the test materials and permission to publish the article.



## References

[1] H.-C. Chao, The Mechanism of Ridging in Ferritic Stainless Steels, Trans. ASM. 60 (1967) 37–50.

[2] T.S.A. H. Takechi, H. Kato, On the Mechanism of Ridging Phenomenon in 17%-Chromium Stainless Steel Sheets, Trans. Jap. Inst. Met. 8 (1967) 233.

[3] R.P. Siqueira, H.R.Z. Sandim, T.R. Oliveira, D. Raabe, Composition and orientation effects on the final recrystallization texture of coarse-grained Nb-containing AISI 430 ferritic stainless steels, Mater. Sci. Eng. A. 528 (2011) 3513–3519. https://doi.org/10.1016/j.msea.2011.01.007.

[4] M. Brochu, T. Yokota, S. Satoh, Analysis of Grain Colonies in Type 430 Ferritic Stainless Steels by Electron Back Scattering Diffraction (EBSD)., ISIJ Int. 37 (1997) 872–877. https://doi.org/10.2355/isijinternational.37.872.

[5] S. Patra, A. Ghosh, J. Sood, L.K. Singhal, A.S. Podder, D. Chakrabarti, Effect of coarse grain band on the ridging severity of 409L ferritic stainless steel, Mater. Des. 106 (2016) 336–348. https://doi.org/10.1016/j.matdes.2016.05.100.

[6] S. Kodukula, T. Ohligschläger, D. Porter, Quantification of the Severity of Ridging in Ferritic Stainless Steel Sheets Using a Profilometric Technique, 61 (2021) 1–7. https://doi.org/10.2355/isijinternational.ISIJINT-2020-137.

[7] P.D. Wu, D.J. Lloyd, Y. Huang, Correlation of ridging and texture in ferritic stainless steel sheet, Mater. Sci. Eng. A. 427 (2006) 241–245. https://doi.org/10.1016/j.msea.2006.04.045.

[8] H.J. Shin, J.K. An, S.H. Park, D.N. Lee, The effect of texture on ridging of ferritic stainless steel, Acta Mater. 51 (2003) 4693–4706. https://doi.org/10.1016/S1359-6454(03)00187-3.

[9] H. Shin, S. Hong, D. Lee, Analysis of ridging in ferritic stainless steel and aluminum alloy sheets, (2004) 11–17.

[10] N.J. Wittridge, R.D. Knutsen, A microtexture based analysis of the surface roughening behaviour of an aluminium alloy during tensile deformation, Mater. Sci. Eng. A. 269 (1999) 205–216. https://doi.org/http://dx.doi.org/10.1016/S0921-5093(99)00145-8.

[11] M.-Y.Y. Huh, O. Engler, Effect of intermediate annealing on texture, formability and ridging of 17%Cr ferritic stainless steel sheet, Mater. Sci. Eng. A. 308 (2001) 74–87. https://doi.org/10.1016/S0921-5093(00)01995-X.

[12] T. TSUCHIYAMA, R. HIROTA, K. FUKUNAGA, S. TAKAKI, Ridging-free Ferritic Stainless Steel Produced through Recrystallization of Lath Martensite, ISIJ Int. 45 (2005) 923–929. https://doi.org/10.2355/isijinternational.45.923.

[13] D. Raabe, K. Lücke, Textures of ferritic stainless steels, Mater. Sci. Technol. 9 (1993) 302–312. https://doi.org/10.1179/026708393790172132.

[14] S. Park, K. Kim, Y. Lee, C. Park, Evolution of Microstructure and Texture Associated with Ridging in Ferritic Stainless Steels., ISIJ Int. 42 (2002) 100–105. https://doi.org/10.2355/isijinternational.42.100.
[15] DEFILIPPI JD, CHAO HC, Effect of chromium and molybdenum segregation on the ridging behavior of type 434 stainless steel, Met Trans. 2 (1971) 3209–3216. https://doi.org/10.1007/bf02814974.
[16] K. SUZUKI, S. ASAMI, K. SUZUKI, Microsegregation of Chromium and Carbon and Ridging Phenomenon in 18Cr Stainless Steel Sheets, Tetsu-to-Hagane. 64 (1978) 1607–1614.
[17] K. SUZUKI, S. ASAMI, K. SUZUKI, Formation of Ridging Related to the Banded Segregation Pattern of Cr and C on Ferritic Stainless Steel Sheet, Trans. Iron Steel Inst. Japan. 23 (1983) 731–737. https://doi.org/10.2355/isijinternational1966.23.731.
[18] K. Suzuki, S. Asami, Ridging Phenomenon Related to the Undulated Segregation-pattern on Transverse Section in Ferritic Stainless Steel, Trans. Iron Steel Inst. Japan. 24 (1984) 359–364. https://doi.org/10.2355/isijinternational1966.24.359.
[19] H. Shibata, S. Itoyama, Y. Kishimoto, S. Takeuchi, H. Sekiguchi, Prediction of Equiaxed Crystal Ratio in Continuously Cast Steel Slab by Simplified Columnar-to-Equiaxed Transition Model, ISIJ Int. 46 (2006) 921–930. https://doi.org/10.2355/isijinternational.46.921.
[20] J. Hutt, D. Stjohn, The origins of the equiaxed zone—Review of theoretical and experimental work, Int. J. Cast Met. Res. 11 (1998) 13–22. https://doi.org/10.1080/13640461.1998.11819254.
[21] J.C. Kim, J.J. Kim, J.Y. Choi, J.H. Choi, S.K. Kim, Control of columnar-to-equiaxed transition in continuous casting of 16% Cr stainless steel, Metall. Ital. 101 (2009) 43–48.
[22] S. Kodukula, M. Petäjäjärvi, J. Savolainen, T. Fabritius, D. Porter, Influence of Calcium Treatment and Electromagnetic Stirring on Ridging in Dual-Stabilized Ferritic Stainless Steels, Steel Res. Int. 2000445 (2020) 1–10. https://doi.org/10.1002/srin.202000445.
[23] F. Gao, Z. Liu, H. Liu, G. Wang, Influence of the finish rolling temperatures on the microstructure and texture evolution in the ferritic stainless steels, 24 (2011) 343–350.
[24] C. Zhang, Z. Liu, G. Wang, Effects of hot rolled shear bands on formability and surface ridging of an ultra purified 21%Cr ferritic stainless steel, J. Mater. Process. Technol. 211 (2011) 1051–1059. https://doi.org/10.1016/j.jmatprotec.2011.01.005.
[25] T. SAWATANI, K. SHIMIZU, T. NAKAYAMA, M. MIYOSHI, The r Values and Recrystallized Textures of Ti Stabilized Low C, N-17%Cr Stainless Steel Sheets, Tetsu-to-Hagane. 63 (1977) 843–854. https://doi.org/10.2355/tetsutohagane1955.63.5_843.
[26] S. Mehtonen, E. Palmiere, D. Misra, P. Karjalainen, D. Porter, Microstructural and Texture Development during Multi-Pass Hot Deformation of a Stabilized High-Chromium Ferritic Stainless Steel, Isij Int. 54 (2014) 1406–1415. https://doi.org/10.2355/isijinternational.54.1406.
[27] C. Lu, Z. Fang, J. Li, Influence of differential speed rolling ratio on the ridging behavior of ultra purified 17%Cr ferritic stainless steel, Mater. Charact. 135 (2018) 257–264. https://doi.org/10.1016/j.matchar.2017.11.049.
[28] S. Patra, Influence of Hot Band Annealing and Cold Rolling on Texture and Ridging of 430 Stainless Steel Containing Aluminum, Mater. Sci. Appl. 04 (2013) 70–76. https://doi.org/10.4236/msa.2013.41009.
[29] P.D. Wu, H. Jin, Y. Shi, D.J. Lloyd, Analysis of ridging in ferritic stainless steel sheet, Mater. Sci. Eng. A. 423 (2006) 300–305. https://doi.org/10.1016/j.msea.2006.02.043.
[30] F. Gao, F. Yu, R.D.K. Misra, X. Zhang, S. Zhang, Z. Liu, Microstructure, Texture, and Deep Drawability Under Two Different Cold-Rolling Processes in Ferritic Stainless Steel, J. Mater. Eng. Perform. 24 (2015) 3862–3880. https://doi.org/10.1007/s11665-015-1689-5.
[31] I. Samajdar, B. Verlinden, P. Van Houtte, D. Vanderschueren, γ-Fibre recrystallization

texture in IF-steel: An investigation on the recrystallization mechanisms, Mater. Sci. Eng. A. 238 (1997) 343–350. https://doi.org/10.1016/S0921-5093(97)00455-3.
[32] J.H. Lee, S.H. Park, M.Y. Huh, Modification of the recrystallization texture by means of cross rolling in ferritic stainless steel sheets, Mater. Sci. Forum. 449–452 (2004) 113–116. https://doi.org/10.4028/www.scientific.net/msf.449-452.113.
[33] W.B. Hutchinson, E. Lindh, P. Bate, M. and P. Canadian Institute of Mining, On the determination of textures from discrete orientation measurements, in: 12th, Int. Conf. Textures Mater., National Research Council (Canada) Research Press; , Montreal, Canada, n.d.: pp. 34–39. https://www.tib.eu/de/suchen/id/BLCP%3ACN038276517.
[34] H.-J. Shin, J.-K. An, S.H. Park, D.N. Lee, The effect of texture on ridging of ferritic stainless steel, Acta Mater. 51 (2003) 4693–4706. https://doi.org/10.1016/S1359-6454(03)00187-3.
[35] C.W. Sinclair, J.D. Mithieux, J.H. Schmitt, Y. Bréchet, Recrystallization of stabilized ferritic stainless steel sheet, Metall. Mater. Trans. A Phys. Metall. Mater. Sci. 36 (2005) 3205–3215. https://doi.org/10.1007/s11661-005-0091-6.
[36] K. Lücke, M. Hölscher, Rolling and Recrystallization Textures of BCC Steels, Textures Microstruct. 14 (1991) 564783. https://doi.org/10.1155/TSM.14-18.585.
[37] M.R. Barnett, J.J. Jonas, Influence of Ferrite Rolling Temperature on Microstructure and Texture in Deformed Low C and IF Steels, ISIJ Int. 37 (1997) 697–705. https://doi.org/10.2355/isijinternational.37.697.
[38] M.Z. Quadir, B.J. Duggan, Shear Band Thickening during Rolling of Interstitial Free Steel, ISIJ Int. 46 (2006) 1495–1499. https://doi.org/10.2355/isijinternational.46.1495.
[39] S. V. Mehtonen, L.P. Karjalainen, D.A. Porter, Hot deformation behavior and microstructure evolution of a stabilized high-Cr ferritic stainless steel, Mater. Sci. Eng. A. 571 (2013) 1–12. https://doi.org/10.1016/j.msea.2013.01.077.
[40] W.B.Hutchinson, Deformation Microstructures and Textures in Steels, Philos. Trans. R. Soc. A Math. Phys. Eng. Sci. 1756 (1999) 1471–1485.
[41] D. Gomes, C. Moreira, D. Alcântara, T. Reis, D. Oliveira, B. Mendonc, The effect of grain size and initial texture on microstructure , texture , and formability of Nb stabilized ferritic stainless steel manufactured by two-step cold rolling, 8 (2019) 4151–4162. https://doi.org/10.1016/j.jmrt.2019.07.024.
[42] T. SAKAI, Y. SAITO, K. KATO, Texture formation in low carbon Ti bearing steel sheets by high speed hot rolling in ferrite region., Trans. Iron Steel Inst. Japan. 28 (1988) 1036–1042. https://doi.org/10.2355/isijinternational1966.28.1036.
[43] M.R. Barnett, J.J. Jonas, Distinctive Aspects of the Physical Metallurgy of Warm Rolling., ISIJ Int. 39 (1999) 856–873. https://doi.org/10.2355/isijinternational.39.856.
[44] J. Hyun Park, D. Sik Kim, S. Lee, Inclusion Control of Ferritic Stainless Steel by Aluminum Deoxidation and Calcium Treatment, Metall. Mater. Trans. B. 36B (2005) 67–73. https://link-springer-com.pc124152.oulu.fi:9443/content/pdf/10.1007/s11663-005-0007-2.pdf (accessed February 19, 2020).
[45] C. Zhang, Y. Xu, L. Zhang, X. Zhou, Crystal Plasticity Analysis of the Relation between Micro-Texture and Surface Ridging for a 21%Cr Ferritic Stainless Steel, Steel Res. Int. 2000109 (2020) 1–12. https://doi.org/10.1002/srin.202000109.

Figures

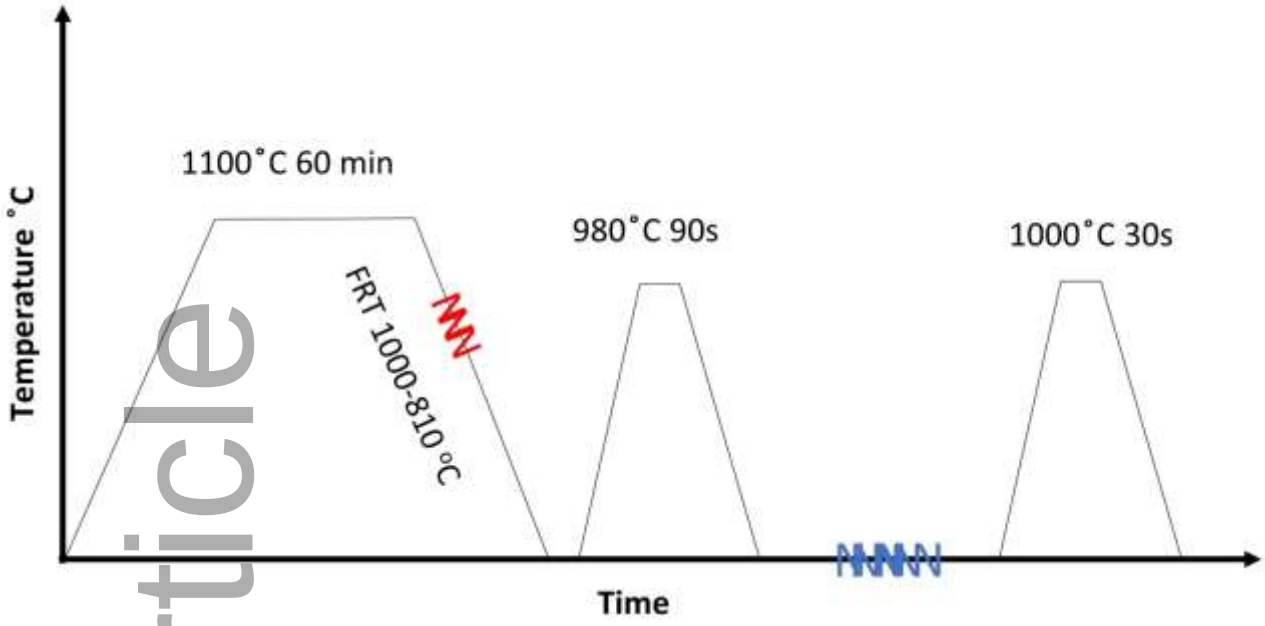


Figure 1. Schematic diagram illustrating the applied thermomechanical processing schedule involving slab re-heating, hot rolling followed by pre-annealing, cold rolling and final annealing.

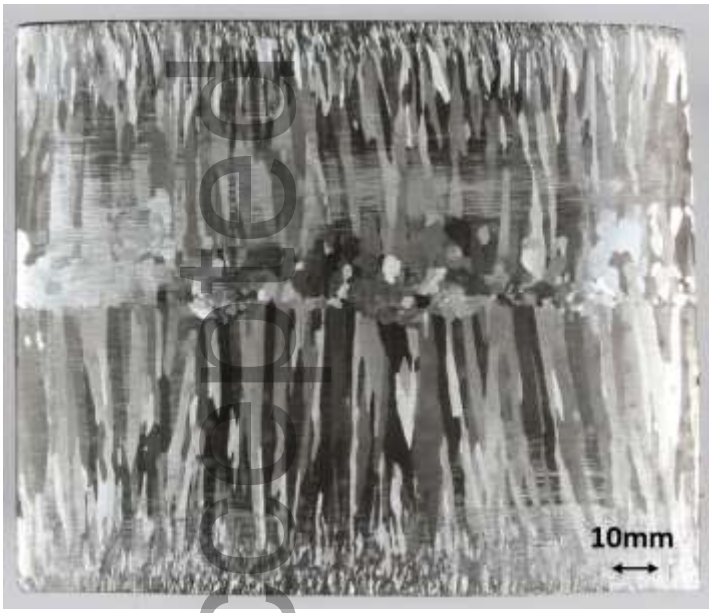


Figure 2. Macro-etched slab cross-section.

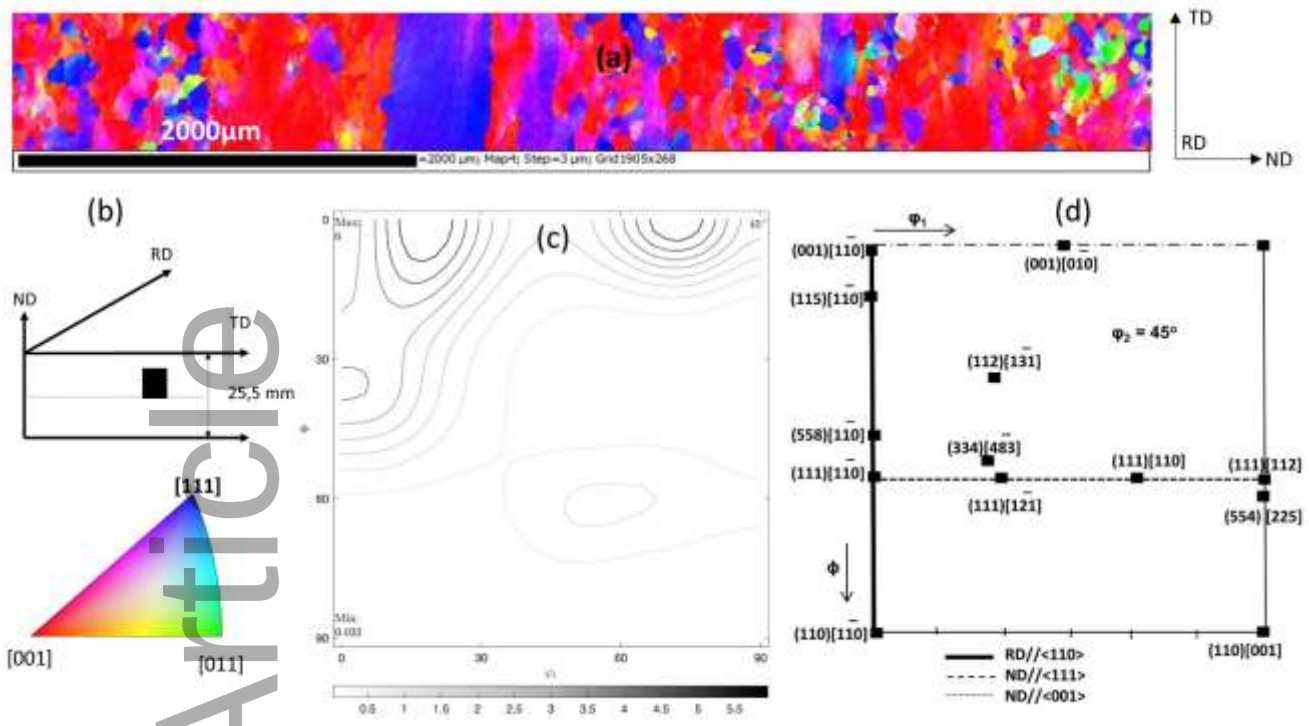


Figure 3. (a) EBSD-IPF image of a TD-ND cross section of the transfer bar in the as-received condition. The scale bar is 2 mm long. (c) The location of the area covered by the EBSD measurements. (c) orientation density function (ODF) of the EBSD-IPF map at $\Phi_2$=45°. Each contour represents a step of 1.
(d) Important orientations on ODF section $\Phi_2$=45°

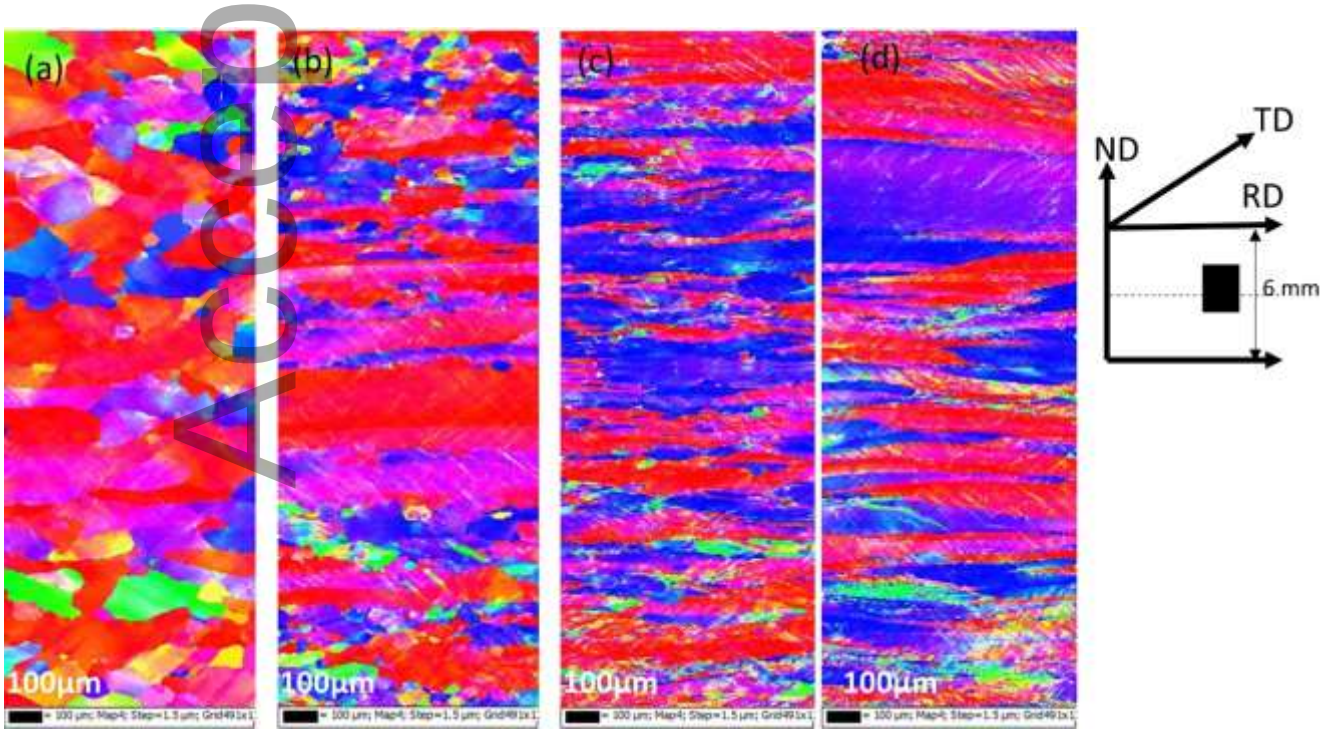

Figure 4. EBSD-IPF images of RD-ND cross sections of the hot rolled samples. FRT: (a) 1000 °C (b) 910 °C (c) 870 °C and (d) 810 °C. The scale bars are 0.1 mm long.

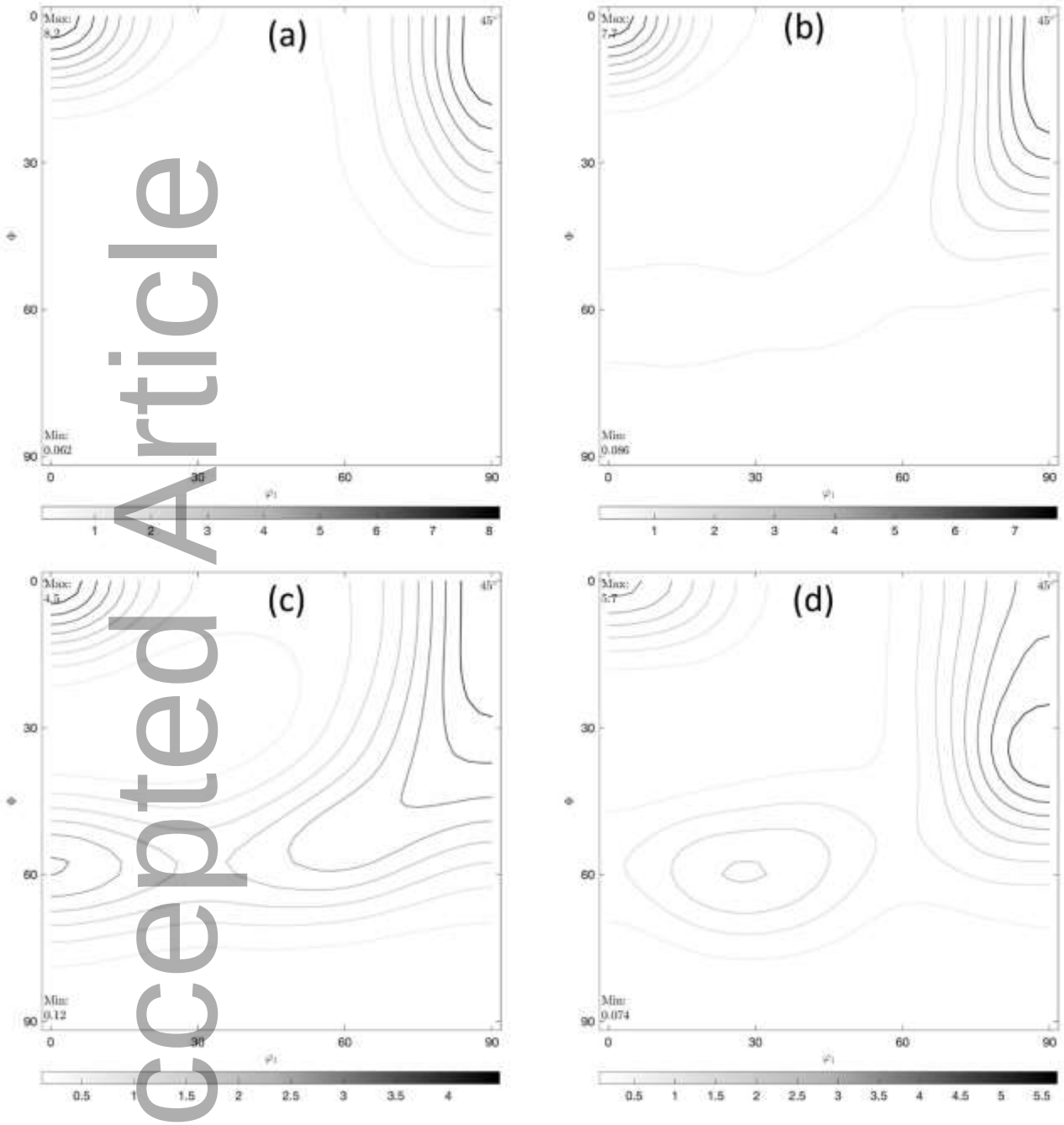




Figure 5. ODF sections of hot rolled samples at $\Phi_2$=45°. FRT (a) 1000, (b) 910, (c) 870 and (d) 810 °C. Each contour represents a step of 1.

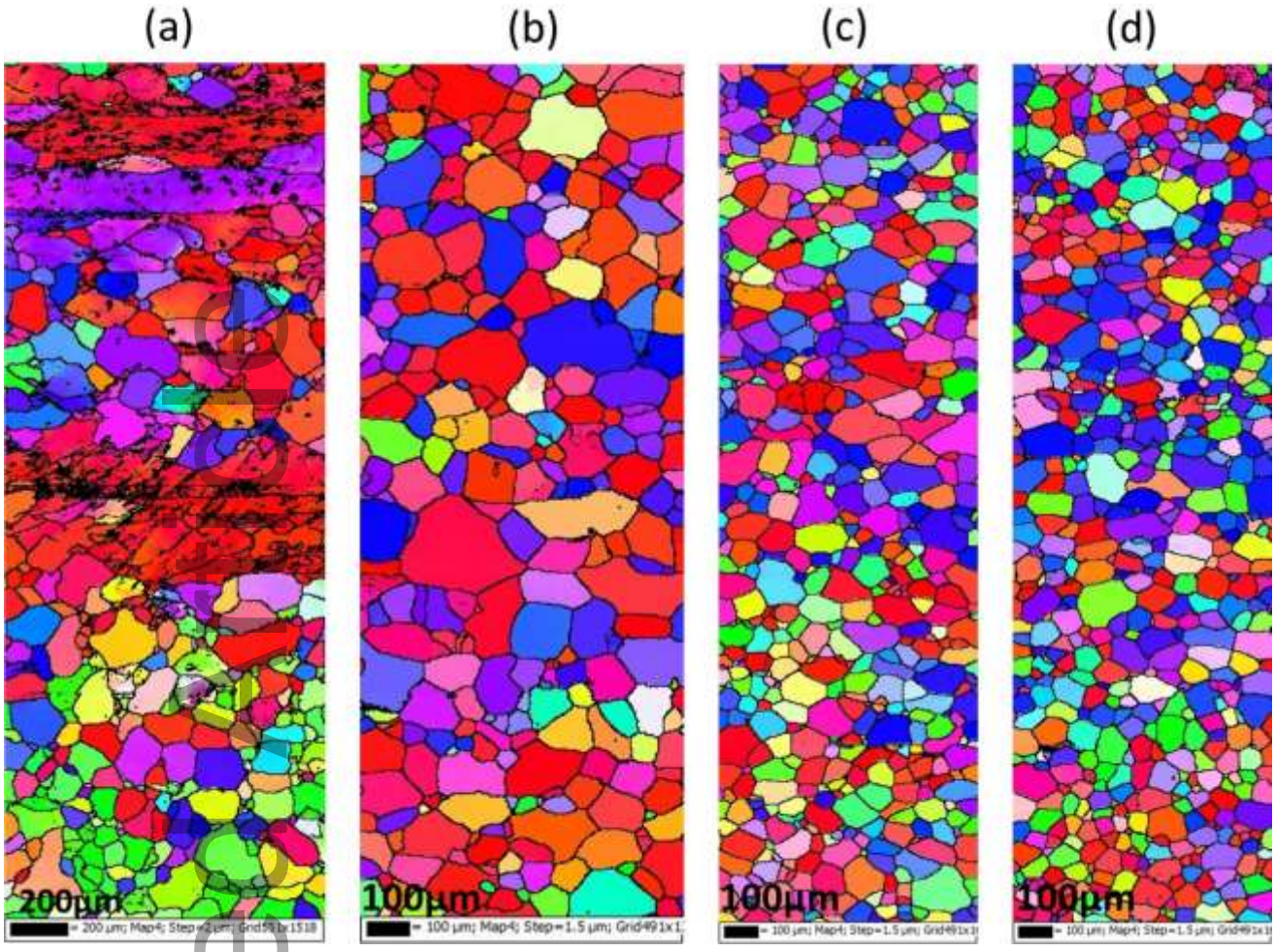


Figure 6. EBSD-IPF images of RD-ND cross sections of the hot rolled annealed (HRA) samples with different hot rolling finishing temperatures at (a) 1000 °C (b) 910 °C (c) 870 °C and (d) 810 °C

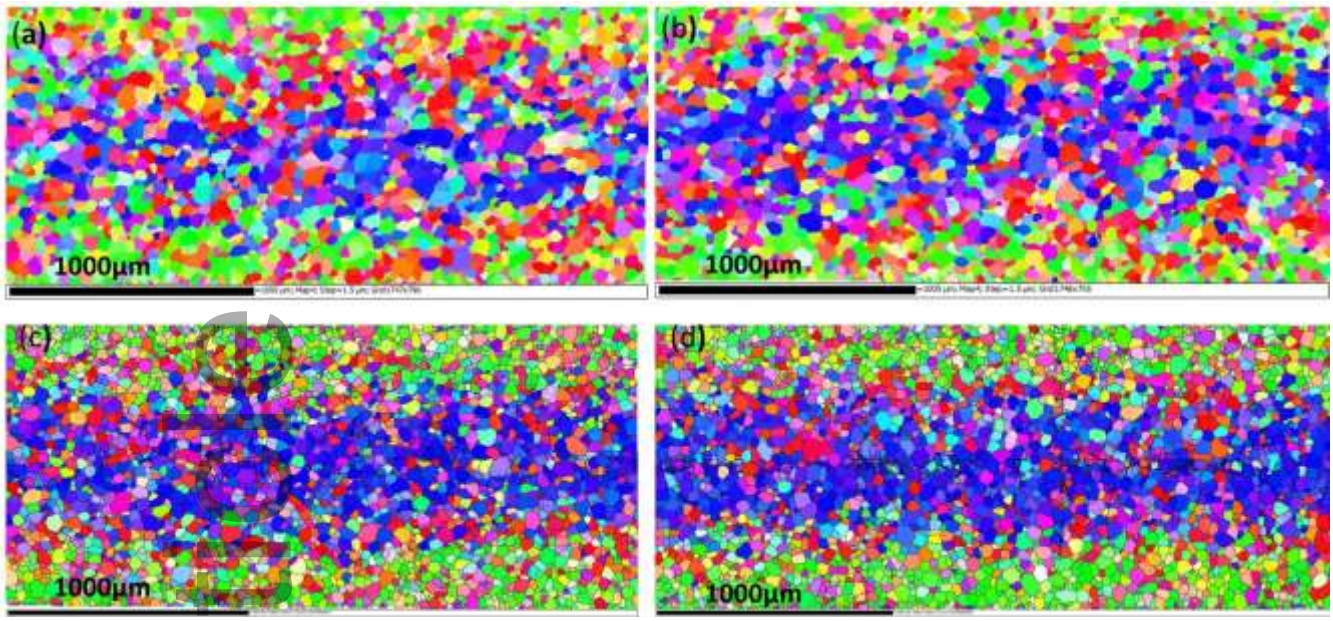


Figure 7. EBSD-IPF images of TD-ND cross sections of the cold rolled annealed (CRA) samples with different hot rolling finishing temperatures at (a) 1000 °C (b) 910 °C (c) 870 °C and (d) 810 °C

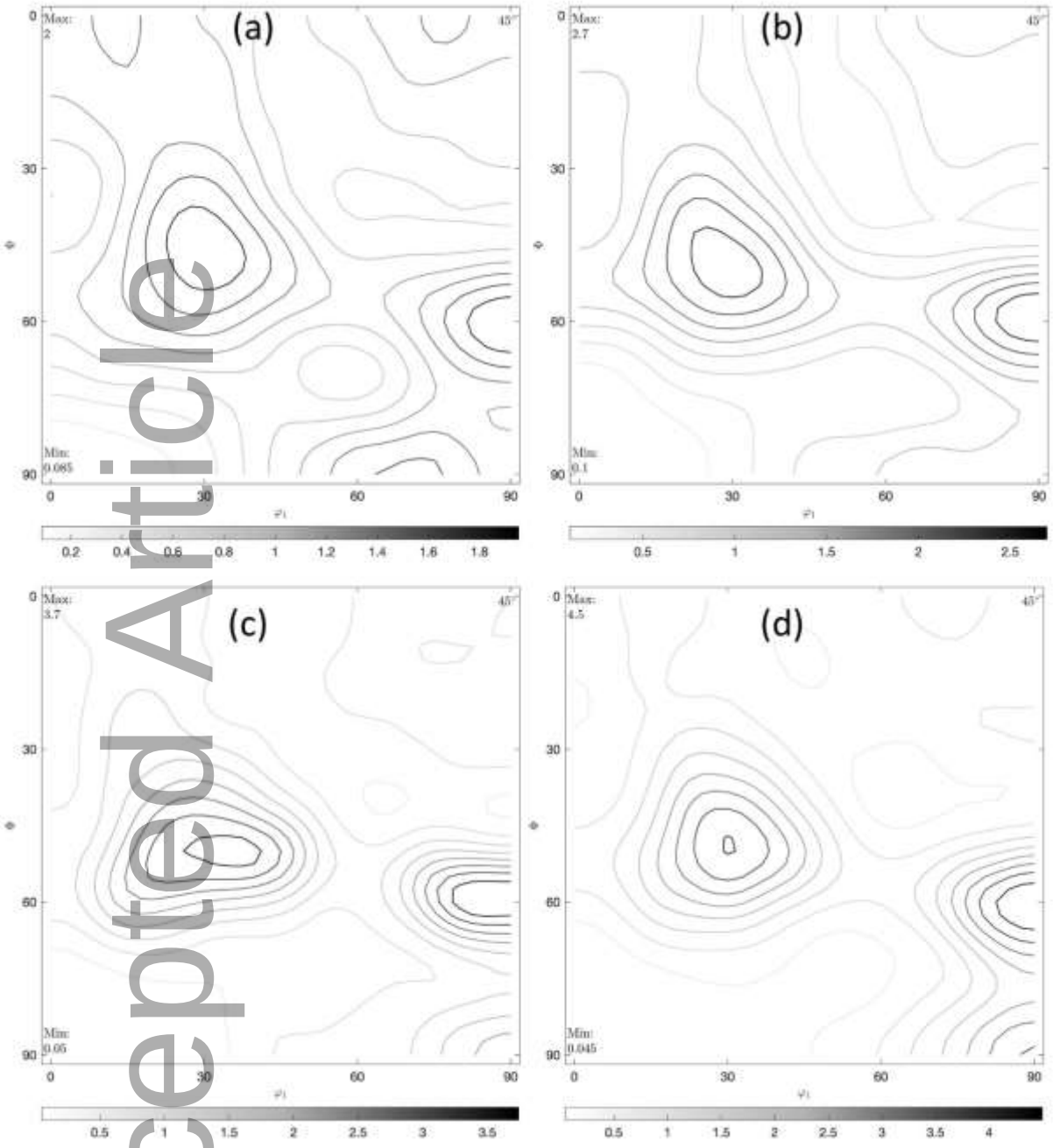


**Figure 8**. $\Phi_2$=45° ODF sections after cold-rolling and annealing. Hot-rolling FRT a) 1000 °C, b) 910 °C, c) 870 °C and d) 810 °C. Each contour represents a step of 1.

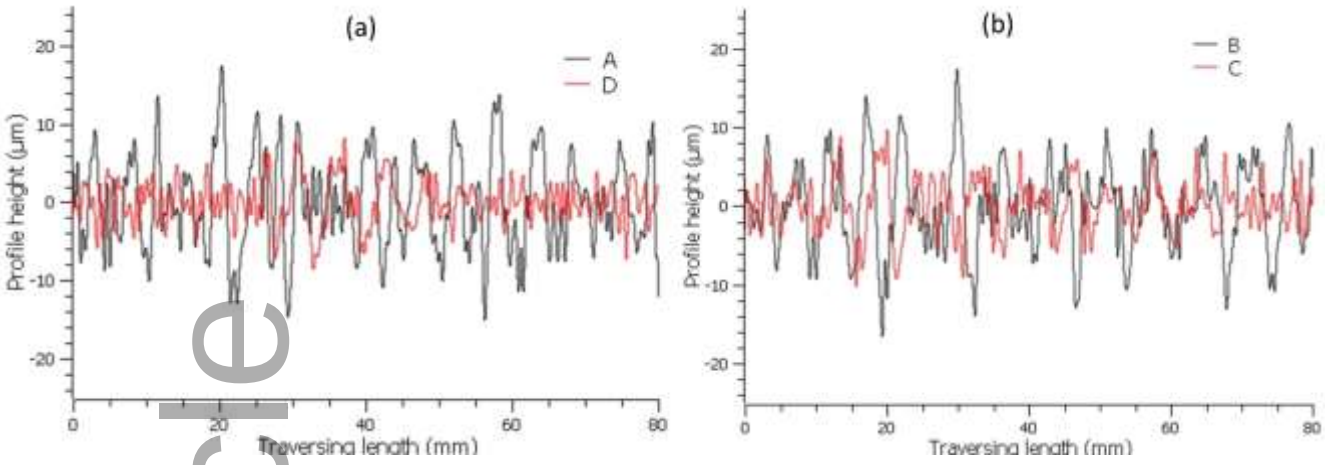


Figure 9. Ridging surface profiles of specimens (a) A and D with FRT of 1000 °C and 810 °C (b) specimen B and C with FRT 910 °C and 870 °C

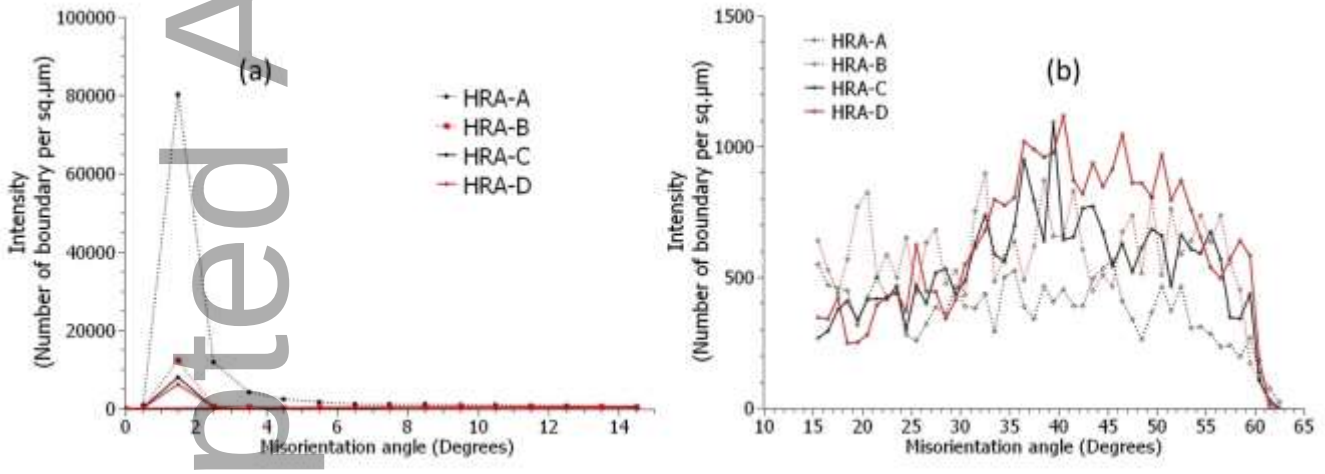


Figure 10. Misorientation profiles after hot rolling and annealing of (a) low angle boundary (2° to 15°) (b) high angle boundary (>15°)

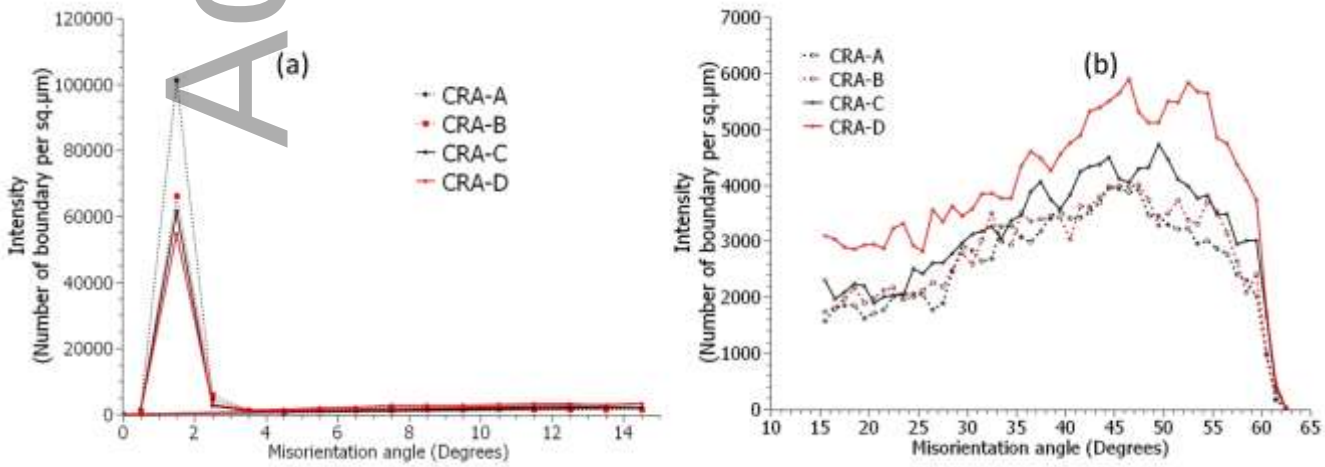

**Figure 11.** Misorientation profiles after cold rolling and annealing of (a) low angle boundary (2° to 15°) (b) high angle boundary (>15°)

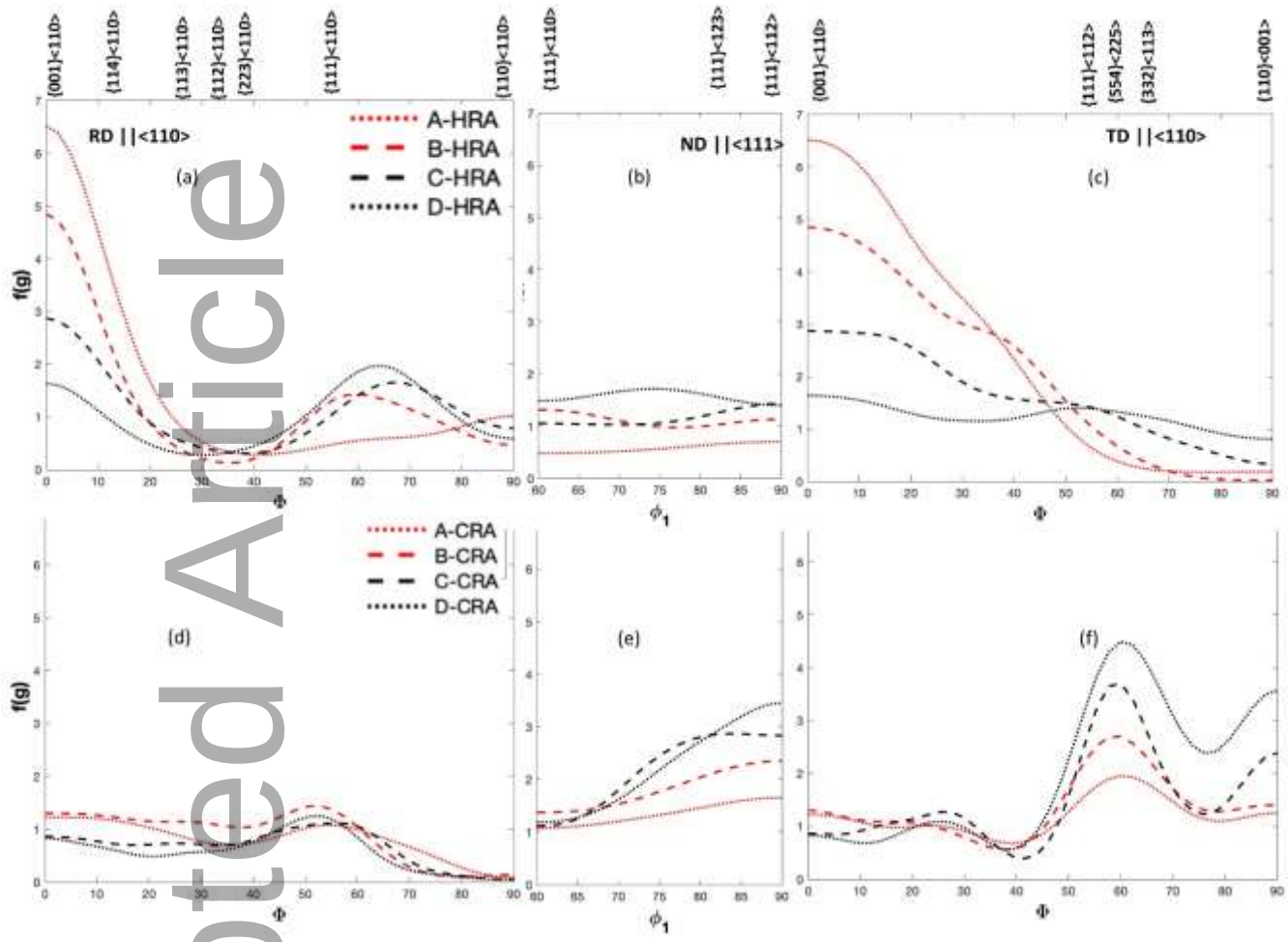


**Figure 12**. Effect of hot-rolling finishing temperature on the intensities of α-fiber ($\varphi_1$ = 0°; $\varphi_2$ = 45° and $\phi$ = 0-90°), , γ- fiber ($\varphi_1$ = 60-90°; $\varphi_2$ = 45° and $\phi$ = 54.7°) and ε- fiber($\varphi_1$ = 90°; $\varphi_2$ = 45° and $\phi$ = 0-90°)
of samples (a-c) in hot rolled annealed condition (d-f) in cold rolled annealed condition.

## Tables

**Table 1**. Chemical composition of the EN 1.4509 steel sample in weight %.

| C | N | Si | Mn | Cr | Ni | Ti | Nb |
|---|---|---|---|---|---|---|---|
| 0.010 | 0.017 | 0.44 | 0.45 | 17.54 | 0.16 | 0.13 | 0.36 |

**Table 2**. Laboratory hot and cold rolling parameters.

| Sample | FRT (°C) | Roller hearth furnace temperature (°C) | Inter-pass time (s) after 1st, 2nd 3rd & 4 | Black hot band thickness (mm) | Cold band thickness (mm) | Cold reduction (%) |
|---|---|---|---|---|---|---|
| A | 1000 | 1190 | 20,20,20,25 | 5.50 | 1.20 | 78.2 |
| B | 930 | 1080 | 18, 20, 20, 25 | 5.61 | 1.23 | 78.1 |
| C | 870 | 1000 | 18,18,20,25 | 5.82 | 1.24 | 78.7 |
| D | 810 | 1000 | 15,15,15,15 | 6.07 | 1.26 | 79.2 |

Table 3. Mechanical properties and surface profile parameters after ridging tests.

| Sample | $Rp_{(0,2)}$ MPa | $R_m$ MPa | $A_g$ (%) | $A_{80}$ (%) | Rz (µm) | Pc | RI (Rz·Pc) |
|---|---|---|---|---|---|---|---|
| A | 278 | 457 | 19.8 | 30.0 | 25.56 | 0.22 | 5.62 |
| B | 282 | 463 | 19.1 | 22.5 | 23.87 | 0.19 | 4.53 |
| C | 280 | 460 | 18.9 | 25.0 | 15.16 | 0.14 | 2.12 |
| D | 282 | 463 | 19.1 | 26.2 | 12.52 | 0.10 | 1.25 |



Keywords: Hot rolling, cold rolling, texture, hot rolling finishing temperature, ridging

Suresh Kodukula*, Heikki Kokkomäki, Esa Puukko, David Porter, Jukka Kömi

Title: Influence of Hot Rolling Finishing Temperature on Texture and Ridging Resistance in Stabilized Ferritic Stainless Steels

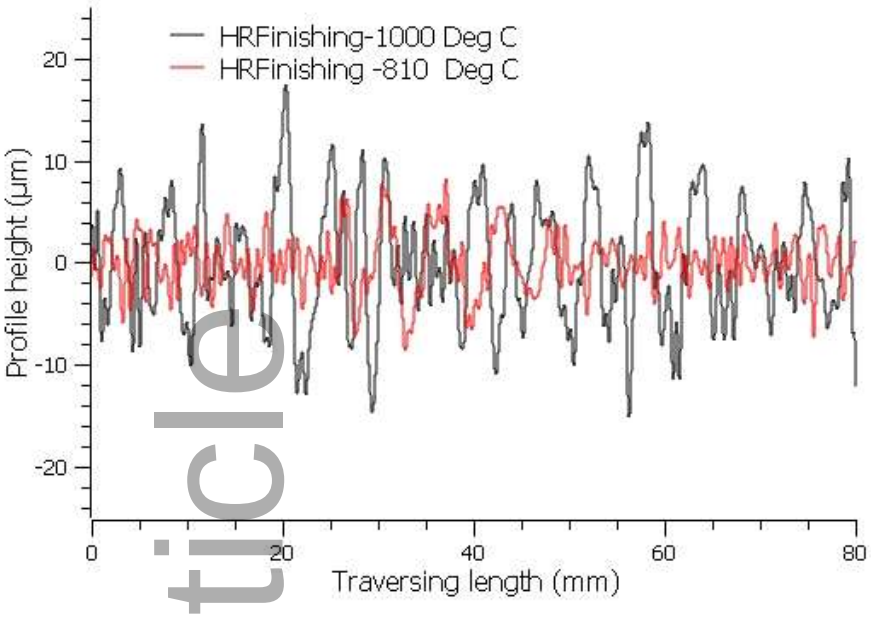




**Short summary:**

The influence of hot rolling finishing temperature on texture and ridging resistance is investigated in dual stabilized (Ti and Nb) ferritic stainless steels. Lowering the hot rolling finishing temperature improved the strengthened the γ-fiber texture in the hot band and further improved the final texture of the cold band which enhanced the resistance to ridging.